Stony Brook University

Morphological Control of Poly(ethylene oxide)/Polystyrene Blend Thin Films by Using Supercritical Carbon Dioxide

A Thesis Presented

by

Xiameng Chen

to

The Graduate School

in Partial Fulfillment of the

Requirements

for the Degree of

Master of Science

in

Materials Science and Engineering

Stony Brook University

May 2012

Stony Brook University

The Graduate School

Xiameng Chen

We, the thesis committee for the above candidate for the

Master of Science degree, hereby recommend

acceptance of this thesis.

Tadanori Koga – Thesis Advisor
Assistant Professor, Materials Science and Engineering

Michael Dudley – Committee Member
Professor, Materials Science and Engineering

T.A. Venkatesh – Committee Member
Assistant Professor, Materials Science and Engineering

This thesis is accepted by the Graduate School

Charles Taber
Interim Dean of the Graduate School

Abstract of the Thesis

Morphological Control in Poly(ethylene oxide)/Polystyrene Blend Thin Films by Using Supercritical Carbon Dioxide

by

Xiameng Chen

Master of Science

in

Materials Science and Engineering

Stony Brook University

2012

Polymer blend thin films have been paid great attention to technological applications including adhesion, coatings, liquid crystal alignment, electronics, optics, biotechnology, and sensors. In this thesis, I investigated the effect of supercritical CO_2 ($scCO_2$) as a green solvent for poly(ethylene oxide)/polystyrene (PEO/PS) blend thin films. We prepared a series of PEO/PS blend thin films with different PEO compositions thickness ranging from 20 nm to 50 nm. As a control experiment, we also processed the same PEO/PS films at high temperature (150 ℃) under vacuum. Comparison of these experimental results by using atomic force microscopy and optical microscopy clarified the significant plasticization effect of $scCO_2$ on the phase separation, crystallization of PEO, and the swelling behavior of PS.

Table of Contents

List of Figures

Chapter 1: Introduction

1.1 Polymer Blend Thin Films

1.1.1 Brief review for thin films

Polymer thin films have been receiving dramatically increasing attention in technological applications include: adhesion, coatings, liquid crystal alignment, electronics, optics, biotechnology and sensors.[1,2] These systems provide many advantages, such as their easier processing, inexpensive cost, control of properties over other materials.[3] But the application of the polymer thin film still has many limitations for the unknown properties.[4] Due to the effects of interfacial interactions, with the free surface and substrate, and finite size effects, the properties of polymer thin films and bulk polymers are quite different, including glass transition temperature, structural stability, diffusion coefficients, and crystallization, viscosity and phase transition temperatures in polymer-polymer mixtures and ordering temperatures in block copolymers.[5]

To know more about the thin film, the morphology of the thin films should be understand. There are many factors affect the film morphology such as film thickness, solvent, molecular weight and substrate.[6] Also when a crystalline polymer is introduced in amorphous polymer, the effect of crystallization may lead to different morphology. So the blend thin film is more complicated than one component thin film. It involves phase separation, wetting process and dewetting process.

1.1.2 Thermodynamics of polymer blends and spinodal decomposition

Different polymers can be combined into a single material and exhibit a wide range of phase behaviors. There are four factors control polymer-polymer phase behavior: choice of monomers, molecular architectures, composition, and degree of polymerization. Composition refers to the overall volume fraction of a component, and in two polymers blend system, it is associated with mass ratio of the two polymers. The degree of polymerization is the number of repeat units (monomers) that compose a polymer chain.[7]

The miscibility of polymer mixtures is decided by the Gibbs free energy in Thermodynamic theories. When the blend components are mixed, the Gibbs free energy is negative:

$$\Delta G_m = \Delta H_m - T\Delta S_m < 0 \qquad (1)$$

Where ΔG_m, ΔH_m, and ΔS_m are the Gibbs free energy, the enthalpy and entropy of mixing at mixing temperature T, respectively.[8] Also, the Flory-Huggins theory could estimate the miscibility of polymer mixtures. The polymer-polymer interaction parameter χ is related to the solubility parameters of the components in the Flory-Huggins approach as follows:

$$\chi = \frac{V_1^0(\delta_1 - \delta_2)^2}{RT} \qquad (2)$$

Where V_1^0 is the molar volume of component 1, and δ_1 and δ_2 are the solubility parameters of two components. T is the mixing temperature. If the interaction parameter χ for the two components is negative, the two polymers are miscible.[9] Values of $\chi_{PS\ PEO}$ and $\chi_{PEO\ PS}$ were calculated to be 0.28 and 0.11.[10] The former value is considered PS as the first component, and the latter one is taken PEO for the first component. So the two values are all positive which means PS and PEO is incompatible.

Polymer PS and Polymer PEO blend films are immiscible and lead to phase separation and various morphologies. Spinodal decomposition is a mechanism of two or more components separating into different phases with different chemical compositions and physical properties. Fig. 1-1 is the phase diagram which illustrates phase transformation and spinodal decomposition in blend system.

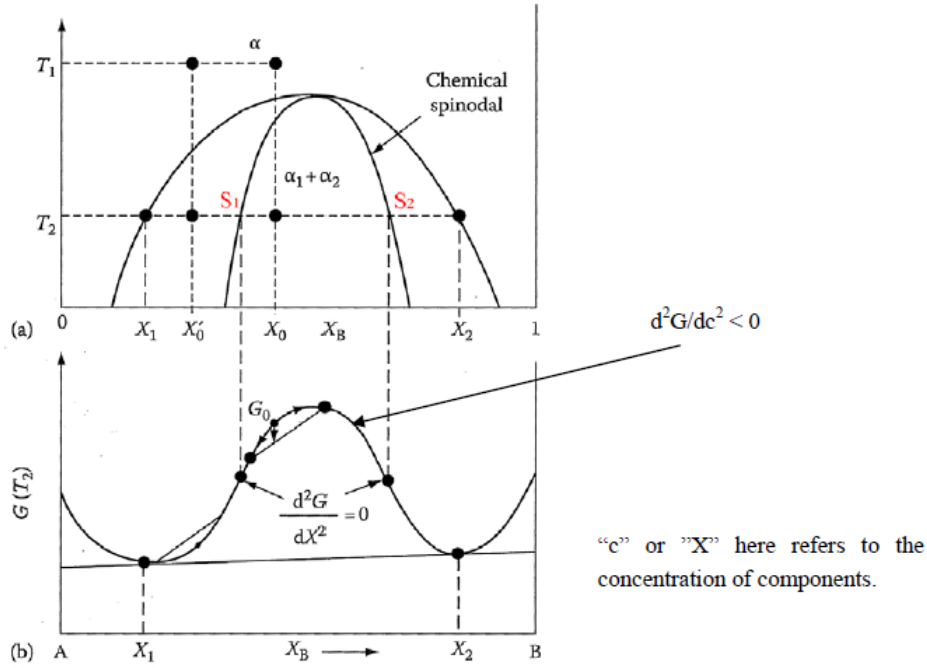

Fig. 1-1 Phase diagram of the two components.

In the phase diagram, phase separation occurs when a material undergoes a transition into the unstable region of the phase diagram and the boundary of the unstable region is referred as the binodal curve. Inside the binodal is a region called the spinodal, where the curvature of the free-energy curve is negative. The binodal and spinodal meet at the critical point. Spinodal decomposition occurs when a material is moved into the spinodal region of the phase diagram. For example, if a material with composition of X_0 heated at a high temperature T_1 and then rapidly cooled to low temperature T_2, the material will be unstable. To decrease the total free energy, A-rich and B-rich regions will be produced by the small fluctuation in composition. In other case, if a material with composition of X_0' is quenched from high temperature T_1 to low temperature T_2, it lies outside the spinodal. The material is metastable and the free energy of the system can be decreased by the nucleating of one component. Therefore outside the spinodal the transformation must proceed by a process of nucleation and growth.[11]

In this research, we choose three competitions of PEO/PS blend systems, 80/20, 50/50, 20/80 respectively. One mass ratio is in the spinodal region, the other two lie outside the spinodal region.

1.2 Supercritical Carbon Dioxide

1.2.1 Supercritical fluids

Supercritical fluids (SCFs) recently increase a lot of attention as alternative solvents. A SCF is defined as any substance at a temperature and pressure above its critical point. Once it is above its T_c, it can no longer be compressed to a liquid. Fig. 1-2 is a typical P-T phase diagram for a compound. The properties of SCFs are like the combination of liquid and gas. It can have the density of liquid and meanwhile have viscosities and diffusion coefficients that like a gas. So it can dissolve many solids and liquids. Also, it is easy to tune the density of a SCF with small changed in pressure and temperature to meet the requirements of the application.[12] Currently, supercritical fluids could be applied in many fields like reaction, polymerization, catalysis, polymer processing and modification, and dry cleaning.

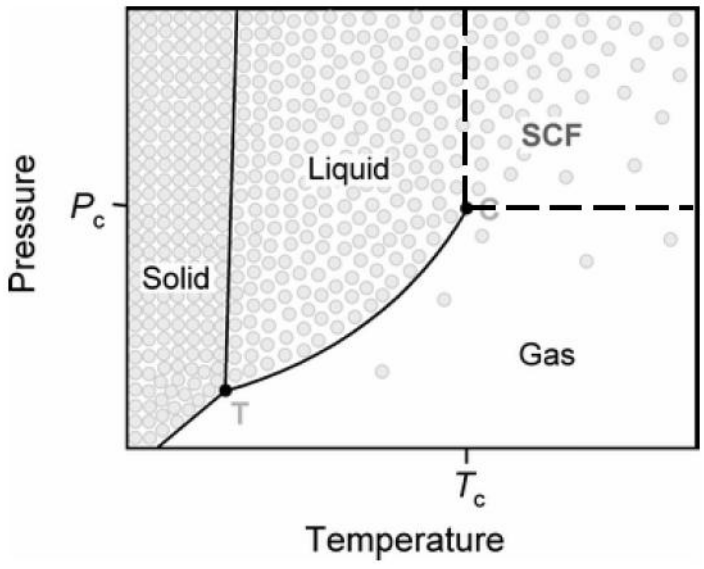

Fig. 1-2 P-T phase diagram of a substance

Among various supercritical fluids, carbon dioxide (CO_2) is the most common material in supercritical application. It has many advantages, firstly, the critical point of CO_2 is 31 ℃ and 7.4 MPa which is accessible to be obtained and also CO_2 is an environmentally solvent as a competitive alternative to toxic organic solvents. And other advantages are like cheap cost price, convenient to process and control, easily separated and recycled by evaporation.[13]

1.2.2 Density fluctuating supercritical carbon dioxide

As CO_2 is above its critical point, it is defined as supercritical carbon dioxide ($scCO_2$) which has the behavior like gas and liquid. $ScCO_2$ may be ideal candidates for use in the development of new chemical processes as solvents depending on its density. It is found that in the vicinity of the solvent's critical point, the solvent density has the greatest change. Large density fluctuations is a special characteristic of SCFs.[14] According to the molecular dynamics simulation of two-dimensional Lennard-Jones fluid, $scCO_2$ is composed of high-density and low-density region result in density fluctuations. As a fluid reaching to its critical point, the correlation length and the isothermal compressibility, κ_T, diverge. Density fluctuations, $\langle(\Delta N)^2\rangle/\langle N\rangle$, are expressed below:

$$\langle(\Delta N)^2\rangle/\langle N\rangle = (N/V)\kappa_T k_B T \quad (3)$$

Where k_B is the Boltzmann constant and T is the thermodynamic temperature. If the κ_T values are known, we can discuss the thermodynamics behavior in density fluctuations based on a series temperature and pressure. Fig. 1-3(a) shows the $\langle(\Delta N)^2\rangle/\langle N\rangle$ values of CO_2 under the isobaric conditions near the critical point. Fig. 1-3(b) is the schematic phase diagram of CO_2 and the solid line represents the ridge of CO_2. From the figure we can see the characteristic features of density fluctuations are (i) in each curve there is a peak, (ii) the amplitude of the fluctuation seems to diverge as approaching the critical point, and (iii) the width of the peak broadens with increasing pressure.[15]

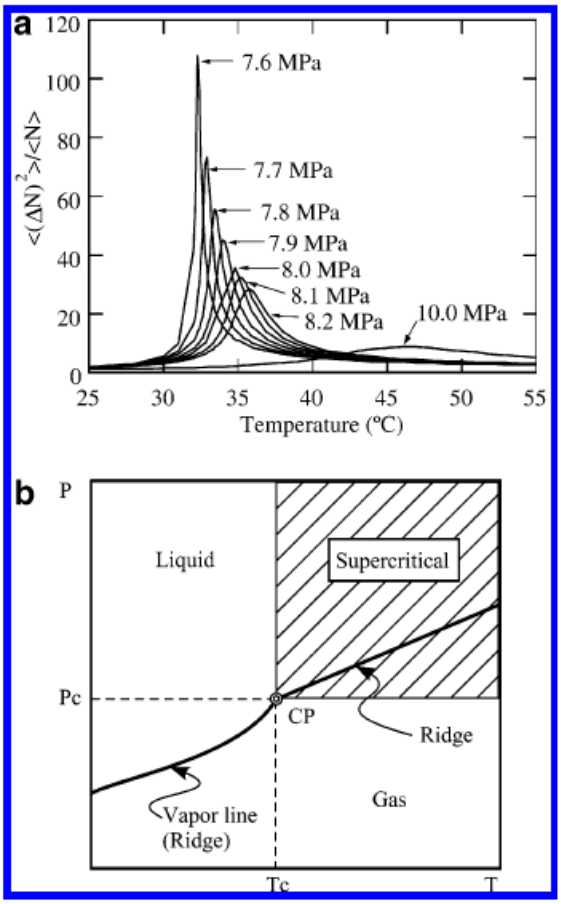

Fig. 1-3 (a) Calculated density fluctuations using the equation of state of CO_2. (b) Schematic phase diagram of CO_2 near the critical point.[15]

It has been found in situ neutron reflectivity (NR) experiments, the large density fluctuations of CO_2 can enhance the swelling behavior of polymer thin films at the density fluctuation ridge even when the miscibility of the polymer with CO_2 is very poor.[16] Fig. 1-4 is the schematic of the scCO_2-based processing for achieving low-density polymer thin films. It consists of two-step procedure: (1) the polymer on the substrate swell due to the density fluctuations in scCO_2, (2) thin film maintain the swollen structures via the quick evaporation of CO_2.[14]

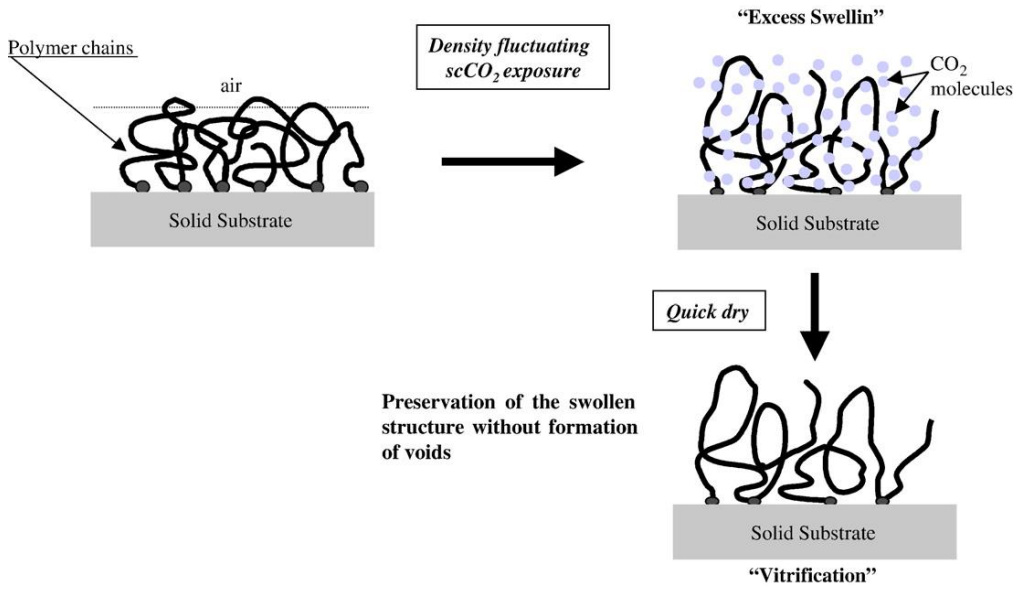

Fig. 1-4 Schematic concept of the $scCO_2$-based processing for achieving low-density polymer thin films.[14]

Except the swelling behavior, $scCO_2$ also has effect on the glass transition temperature (T_g) of polymer. The absorption of CO_2 into polymers results in the reduction of T_g act as plasticization. The T_g depression is related to the concentration in the polymer.[17]

In this research, we will explore the effect of $scCO_2$ on the morphology of blend thin films at ridge conditions and analyze the crystal behavior of PEO in the blend system.

1.3 Effects of CO_2 on Polymer Blend Thin Films

Superctitical carbon dioxide is a 'green' solvent for many applications. Due to the large density fluctuation, $scCO_2$ has effect on the swelling of polymer and the reduction in the glass transition temperature. Except the application as plasticization, the improvement of $scCO_2$ on the miscibility of blend system increases much attention.

Zhou et al.[18] have researched on the surface structure and phase morphology development of PMMA/PS blend thin films with different mass ratio treated with supercritical CO_2 and measured by AFM and phase contrast microscope. They found that after exposing in $scCO_2$, in the surface of the film, the PMMA-rich phase falling down to substrate and PS-rich phase going up to air surface by tuning the treatment temperature and pressure of $scCO_2$. And also, they found a critical phase structure transition temperature/pressure.

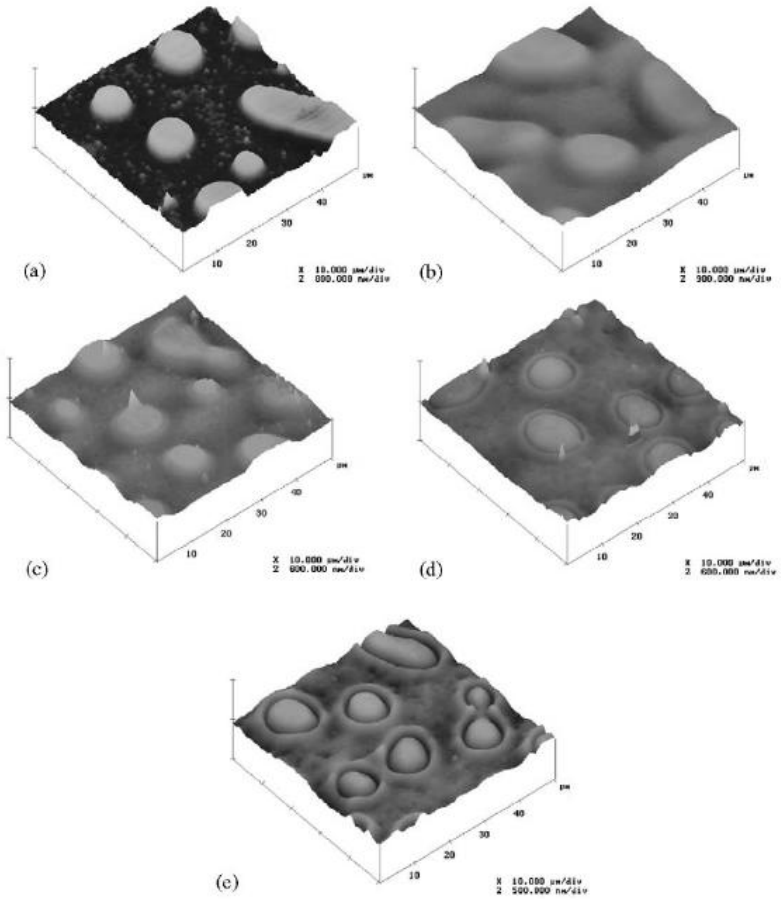

Fig. 1-5 Three-dimensional AFM images ($50 \times 50 \mu m^2$) of PMMA/PS (50/50 w/w) blend thin films treated for 2h in $scCO_2$ (20 MPa) at different temperatures (a) right after preparation,(b) 40 ℃, (c) 50 ℃, (d) 60 ℃, (e) 70 ℃.[18]

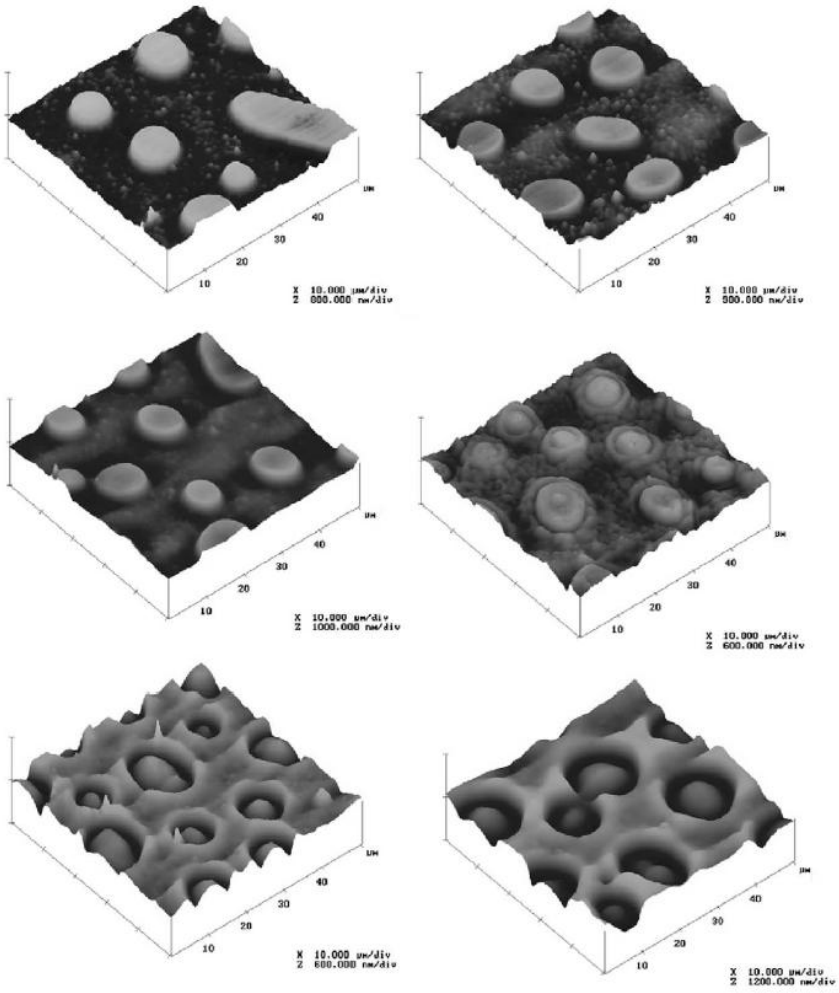

Fig. 1-6 Three-dimensional AFM images ($50\times50\mu m^2$) of PMMA/PS (50/50 w/w) blend thin films treated for 2h in $scCO_2$ (70 ℃) at different pressures (a) right after preparation,(b) 5 MPa (near supercritical), (c) 10 MPa, (d) 20 MPa, (e) 30 MPa, (f) 40 MPa.[18]

Koga et al.[19] have investigated an effect of CO_2 sorption on the compatibility of immiscible polystyrene (PS) and polybutadiene (PB) bilayers by using in situ neutron reflectivity. They found that the excess CO_2 were absorbed to both top PS and bottom PB layers when the bilayers were exposed to CO_2 near the ridge condition of $scCO_2$. Furthermore, they verified that the excess CO_2 increased the interfacial width between the two layers which indicating that $scCO_2$ had a cosolvent effect on immisible thin polymer blend films. Fig. 1-7 Pressure dependence of interfacial width for PS/PB blend thin films at 36 ℃.

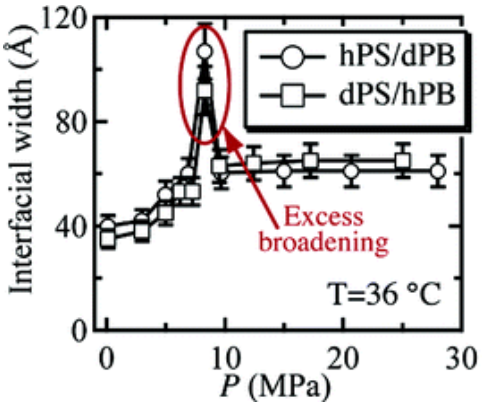

Fig. 1-7 Pressure dependence of interfacial width for hPS/dPB and dPS/hPB ("d" and "h" are deuterium and hydrogenated polymers) blend thin films at 36 ℃.[19]

1.4 Motivation and Objectives

Poly(ethylene oxide) (PEO) and poly(ethylene glycol) (PEG) are amphiphilic and soluble in water as well as in many organic solvents like toluene, acetone, and chloroform.[20] PEO could be applied in electrolytes, biomaterial application, and pH-sensitive sensors.[21] In polymer-based solid electrolytes, PEO could dissolve high concentrations of a wide variety of salts using alkali salts to form polymeric electrolytes.[22] In biomaterial applications, PEO could be used for drug delivery, tissue engineering scaffolds, surface functionalization, and other application.[23] Unfortunately, the crystallization of PEO limits these applications in these fields which need reasonable mechanical properties and electronic properties.[21] Hence we introduce polystyrene (PS) into PEO thin film to control the crystallization behavior.

In this research, the main objective is to control the morphologies of PS/PEO blend thin films. As mentions above, PEO and PS are incompatible polymer blends. Thus, we introduce $scCO_2$ as a co-solvent for the blend thin films and discuss the effect of density fluctuating $scCO_2$. We prepared a series of PEO/PS blend films with different PEO mass ratios (100 %, 80 %, 50 % and 20 %) and thicknesses (20 nm and 50 nm). Based on atomic force microscopy and optical microscopy results, we highlight the differences in the crystallization and the phase separation of the blend films observation before and after the $scCO_2$ process. We show that density fluctuating $scCO_2$ near the critical point induces the largest swelling behavior and the improvement of the miscibility of blend films.

Chapter 2: Morphology of PEO/PS Blend Thin Films with Different PEO Mass Fractions

2.1 Introduction

It is found that addition of an amorphous polymer to a crystalline polymer film results in significant differences in the crystallization process and crystal morphology relative to the pure crystalline polymer thin film. Ferreiro et al.[24] investigated thin blend films of poly(ethylene oxide) (PEO) and poly(methyl methacrylate) (PMMA). They found the morphologies of the PEO changed over a wide range of the PEO mass fractions. Figure 2-1 shows the morphologies as a function of the polymer composition. With increasing the PMMA concentration, three-morphological were observed: spherulite, seaweed dendrite, and well-formed symmetric dendrites.

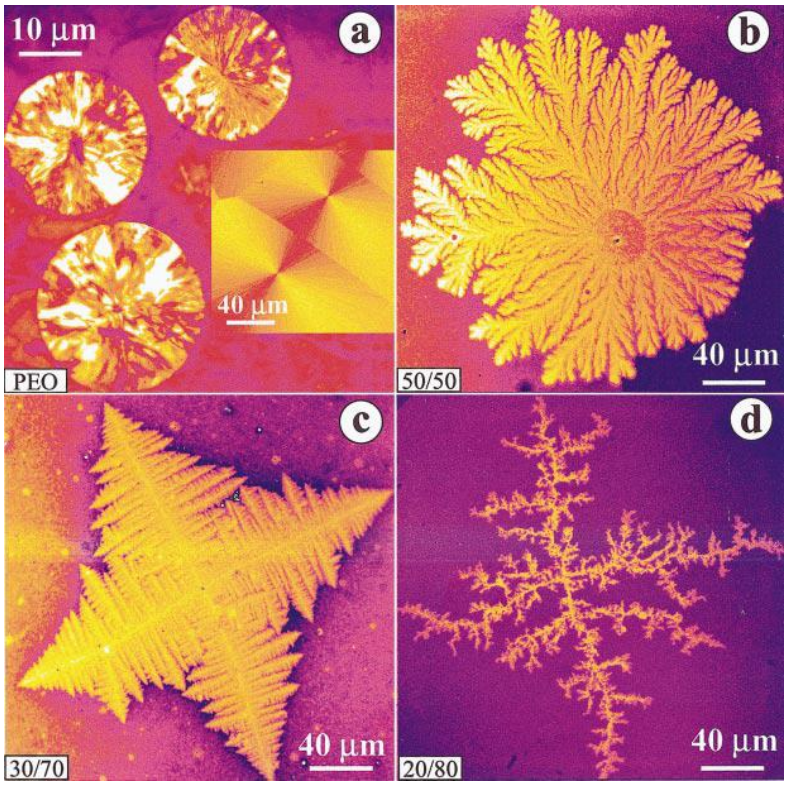

Fig. 2-1 Polymer crystallization morphologies as a function of polymer composition. (a) Spherulitic crystallization of a pure PEO film. (b) Seaweed dendritic growth in a PEO/PMMA (50/50) film. (c) Symmetric dendritic growth in a PEO/PMMA (30/70) film. (d) Fractal dendritic growth in a PEO/PMMA (20/80).[24]

Ma et al.[25] reported the morphological evolution in the blend thin film of polystyrene /poly(ε-caprolactone) (PS/PCL) via AFM. They found that by changing solution concentrations, different kinds of crystal morphologies were observed, such as finger-like, dendritic, and spherulitic-like constructed in the PCL layer. In addition, different film thicknesses lead to different morphological evolution processes and the transformation of dewetting mechanisms. Fig.2-2 shows the schematic presentation of the evolution of dewetting and crystal morphologies.

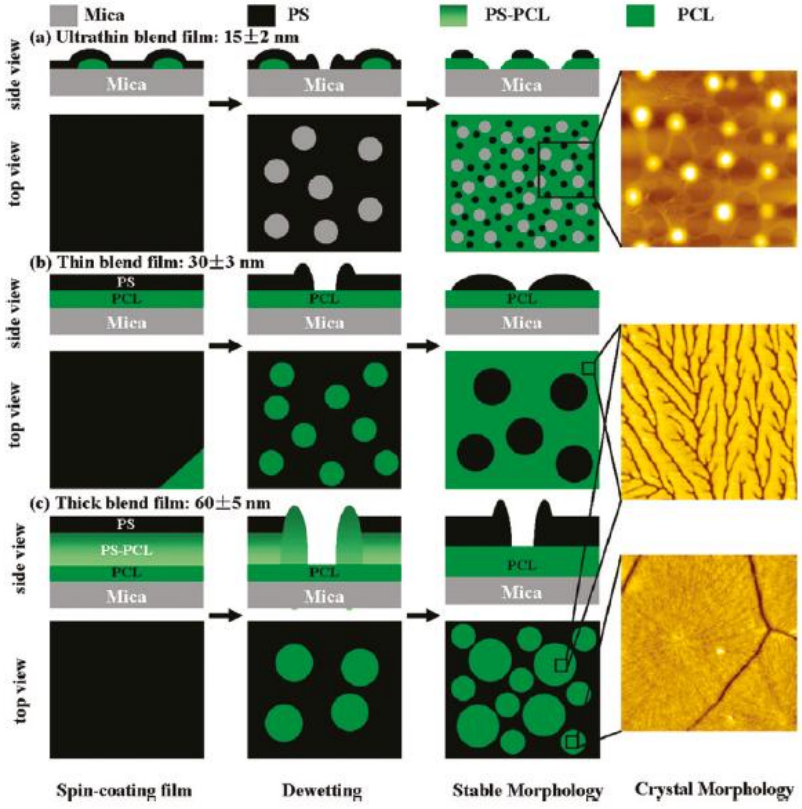

Fig. 2-2 Schematic representation of the evolution of dewetting and crystal morphologies during annealing and crystallization at room temperature for PS/PCL (50/50 wt.) blend films with different thicknesses: (a) 15 nm thick; (b) 30 nm thick; (c) 60 nm thick films.[25]

Thus, we can clearly see that both the film thickness and the mass ratio of the one polymer influence the crystallization morphologies, phase separation, and dewetting process. For this study, we investigate the morphologies of PEO/PS blend system with different polymer mass ratios and film thickness.

2.2 Experimental Section

Material. Poly(ethylene oxide) (PEO) with a number-averaged molecular weight (Mn) of 20,000 was purchased by Sigma-Aldrich. Polystyrene (PS) with Mn=290,000 and a polydispersity index of 1.06 was purchased by Pressure Chemical co. Toluene of ≥ 99.5 % purity (Sigma-Aldrich) was used.

Solution preparation. 20 nm ultrathin blend films are made by a polymer concentration of 0.65 wt% solution. Two polymers were first dissolved in toluene separately, and then mixed together as a blend solution. For different PEO and PS mass competitions of 80/20, 50/50, and 20/80 were used. 50 nm thick blend films were prepared by polymer concentration of 1.44 wt% solution. For different PEO and PS competitions of 80/20, 50/50, and 20/80 were used.

Substrate preparation. Silicon wafers were used as the film substrates. To prepare the substrate, we cleaved the silicon wafer as 1.5 cm*1.5 cm and then used deionized water to wash the wafer. To remove the organic contaminants, first we placed wafers in a solution with a mixture of H_2O:NH_4OH:H_2O_2=1:1:1 at T=150 ℃ for 20 min and rinsed with deionized water, and then placed in H_2O:H_2SO_4:H_2O_2=1:1:1 solution at T=150 ℃ for 20 min and rinsed with deionized water. Finally, they were etched by a HF:H_2O=1:7 solution to remove the native oxide layer.

Spin casting ultrathin films. The ultrathin films were prepared on silicon wafers by a spinner (Head way Research. Lnc, Sarland, Texas) at a rotational speed of 2500 rpm for 30 s.

Conventional method-annealing. After spin-coating, the thin films were annealed the samples in a vacuum oven at 150 ℃ for 2 h.

Elliposometry. We used Rudolph Research Ellipsometer to measure the thickness of PEO/PS blend thin films. The refraction indexes of PEO and PS are 1.455 and 1.589 respectively. For the blend thin films, we calculated the refraction indexes as a function of the mass ratio.

Optical Microscope. To observe the large surface morphology, we used Olympus System Microscope BH2-UMA.

2.3 Results and Discussion

2.3.1 Morphology of 20 nm thick PEO/PS blend films with various PEO mass ratios.

We annealed the 20 nm thick PEO/PS blend film with different mass ratios at 150 ℃ for 2 h and subsequently quenched to room temperature to induce the crystallization. The melting temperature of PEO is 63 ℃ and the glass transition temperature of PS is 100 ℃. Hence, both PEO and PS are melt at T=150 ℃. For the pure PEO film, we annealed at 85 ℃ for 2 h and subsequently quenched in room temperature.

Fig. 2-3 indicates changes in the surface morphologies with different PEO/PS ratios for the 20 nm thick films. In the case of pure PEO, only one phase was observed and the crystal structure was fiber-like. With increasing the concentration of PS, phase separation occurs. Fig. 2-3(c) shows the AFM image for PEO/PS with the mass ratio of 80/20. The bright spherical particle is PS islands and the PEO corresponds to the dark area. When composition becomes symmetric, no clear crystal structures are observed (Fig. 2-3(e,f)). In Fig. 2-3(e), we can see the phase-separated structures, whose domain spacing is the order of 1 μm. According to the friction image shown in Fig.2-3(f), the two regions have different fictions. It is not conclusive, but we believe that the softer bottom layer is PEO, based on the structures formed in the bottom layer, that is similar to those in the 50/50 sample. This is consistent with the fact that the interfacial energy between PEO and Si is lower than that between PS/Si. At the PEO/PS (20/80) composition, the large dendritic crystal structures are seen.

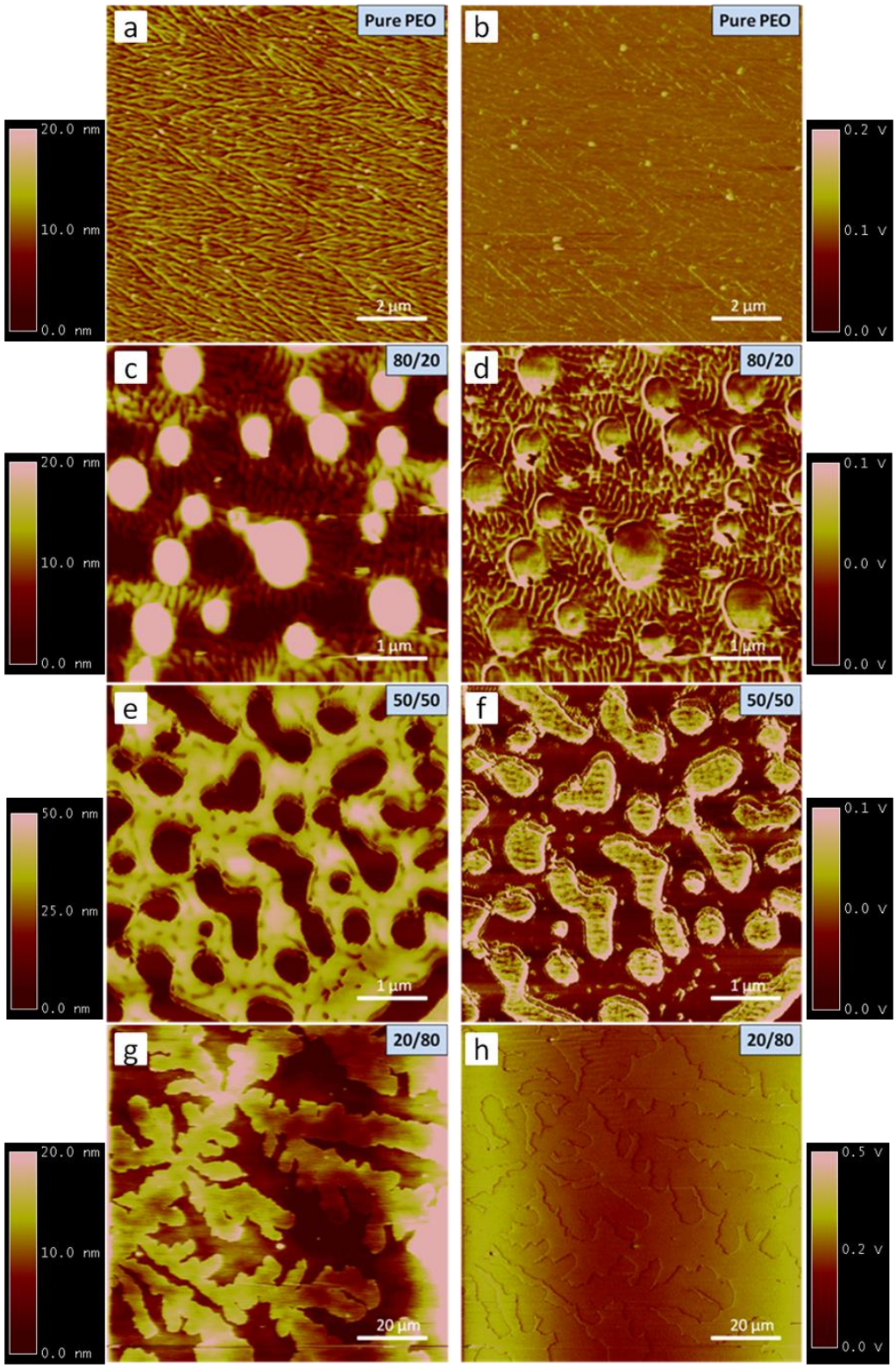

Fig. 2-3 Height images of 20 nm blend film surface morphologies of different PEO/PS mass ratio. (a) Pure PEO, (c) PEO/PS film (80/20), (e) PEO/PS film (50/50), (g) PEO/PS film (20/80). Corresponding AFM friction images of (b) Pure PEO, (d) 80/20, (f) 50/50, (h) 20/80.

2.3.2 Morphology of 50 nm thick PEO/PS blend films with various PEO mass ratios.

Fig. 2-4 is the AFM images of the PEO/PS 50 nm thick films with different PEO mass ratios. The blend films were annealed at 150 ℃ for 2 h and quickly quenched to room temperature. As seen in the 20 nm blend films, the surface topographies change with decreasing the PEO mass ratio. But compared to the 20 nm thick films, no obvious crystal structures are seen even at (20/80) and (80/20) compositions. In the 50/50 blend film, there still have holes at the film surface and the holes are much larger than those seen in the 20 nm thick film. Based on the friction image shown in Fig.2(f), the hole may correspond to the Si substrate, implying that the film may dewet. For the PEO/PS (20/80) sample, there exist small holes at the surface. But these holes do not correspond to the Si substrate, based on the corresponding friction image (Fig. 2(h)).

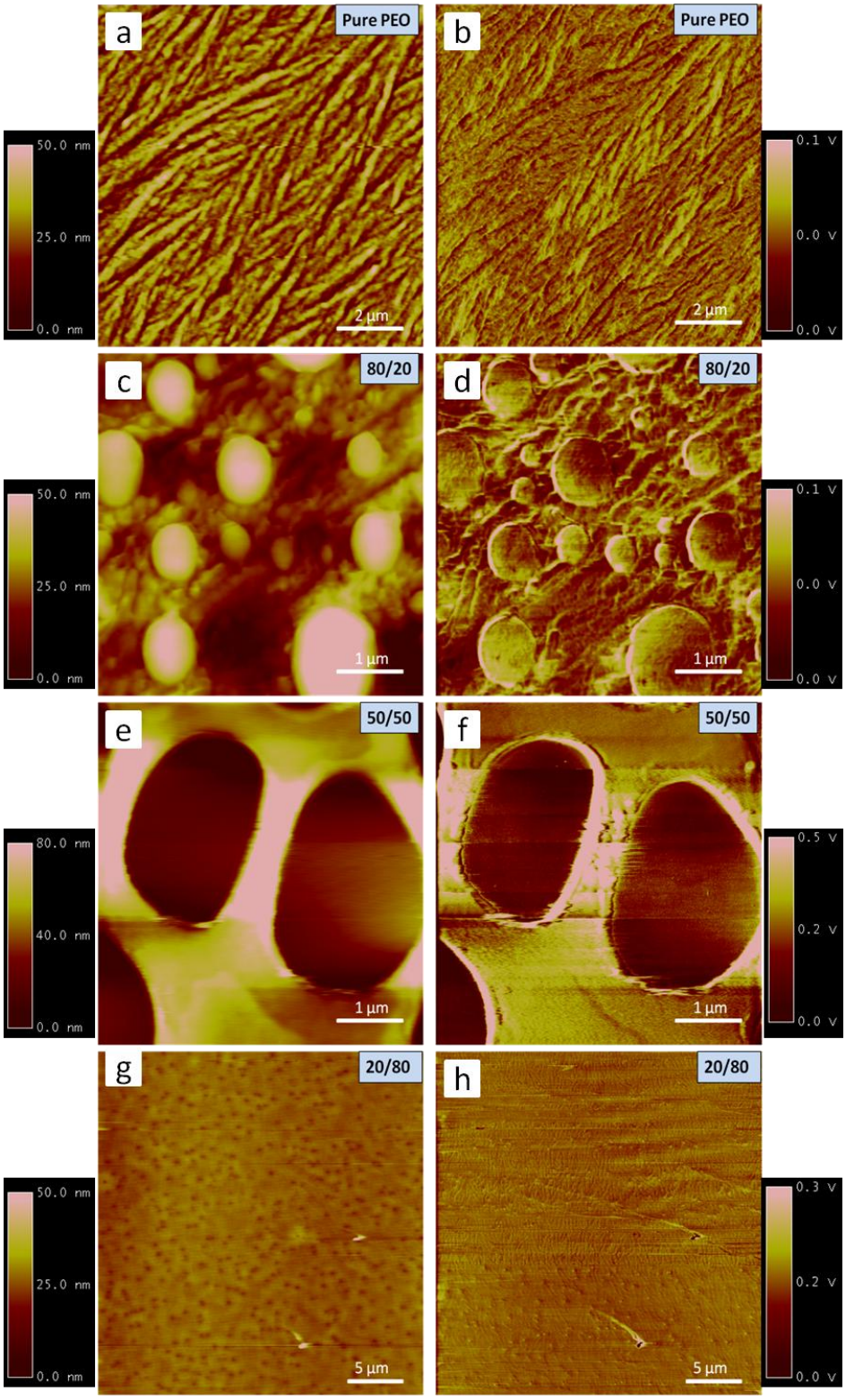

Fig. 2-4 Height images of 50 nm blend film surface morphologies of different PEO/PS mass ratio. (a) Pure PEO, (c) PEO/PS film (80/20), (e) PEO/PS film (50/50), (g) PEO/PS film (20/80). Corresponding AFM friction images of (b) Pure PEO, (d) 80/20, (f) 50/50, (h) 20/80.

Chapter 3: The $ScCO_2$ Effect on PS/PEO Blend Thin Films

3.1 Experimental Section

Our $scCO_2$ processing equipment consist of pressure valves, gauges, a pressure generator, and a main high-pressure chamber (Fig. 3-1).[26] First, we put samples in the chamber, then we used hand-operated syringe pump to load the CO_2 gas into the chamber. The temperature is controlled by a bath circulator within ±0.2 ℃. The pressure stability was within 1 % at given pressure. The films were kept in the chamber for 2 h, and we then released the gas quickly (~20 s) There are two CO_2 conditions used in this research: one is T=36 ℃ P=7.9 MPa, the other is T=50 ℃ P=10 MPa, both of which correspond to the density fluctuation ridge, where the anomalous plasticization effects on polymer thin films has been reported by our research group[27].

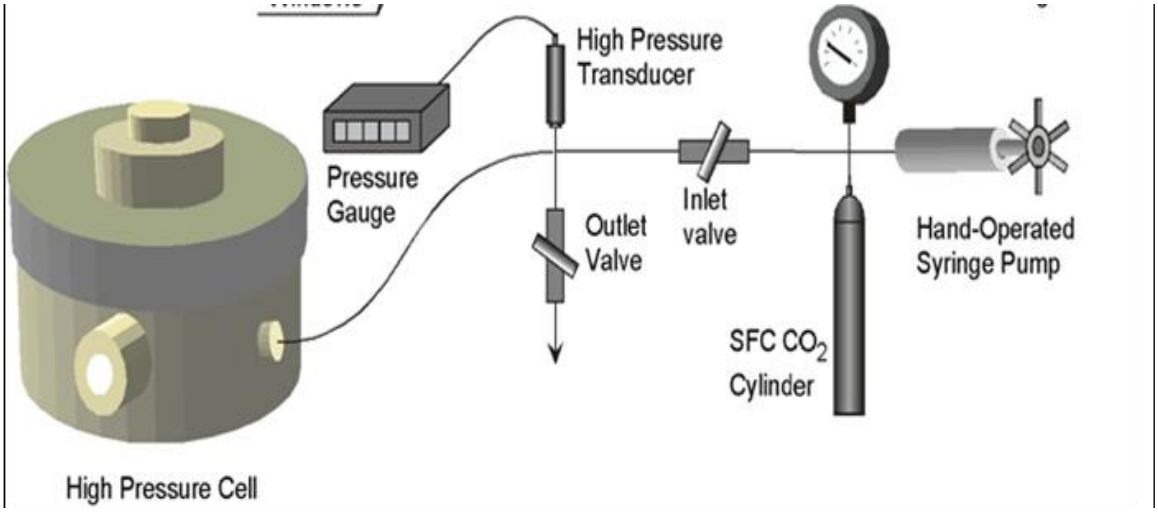

Fig. 3-1 Supercritical carbon dioxide systems.

3.2 Results and Discussion

3.2.1 The effect of $scCO_2$ on the 20 nm PEO/PS blend films

We compared three different conditions for the PEO/PS blend films: (i) annealed at 150 ℃ for 2 h and quenched rapidly to room temperature; (ii) exposed to $scCO_2$ at T=36 ℃ P=7.9 MPa for 2 h and then rapidly quenched; (iii) exposed to $scCO_2$ at T=50 ℃ P=10 MPa for 2 h and then rapid quenched.

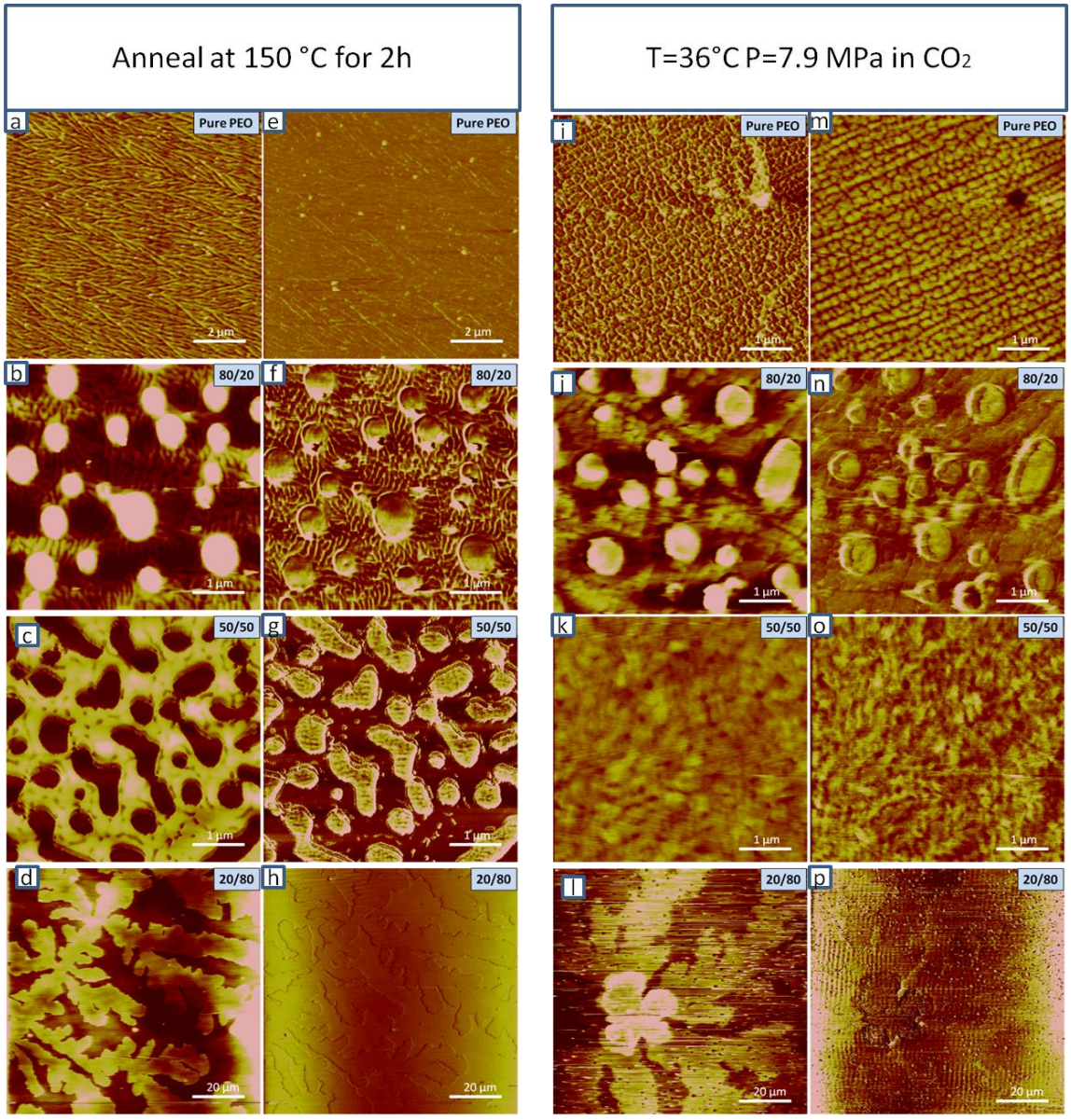

Fig. 3-2 Morphologies of 20 nm ultrathin films in two conditions with four kinds of mass ratios. (a-d) PEO mass fractions are 100 %, 80 %, 50 %, 20 % respectively after annealing for 2 h fast quench. (e-h) Corresponding AFM friction images of (a-d). (i-l) PEO mass ratios are 100 %, 80 %, 50 %, 20 % respectively in the condition of $scCO_2$ at T=36 ℃ and P=7.9 MPa. (m-p) Corresponding AFM friction images of (i-l).

We annealed the blend thin films at T=150 ℃ and quickly quenched to room temperature. With this condition, PEO recrystallized at room temperature from melt, while phase separation and dewet process may occur at high temperature due to the immiscibility of PEO/PS blend films. In Fig. 3-2 we compared two conditions, one is after annealing under vacuum, and the other is after exposure to $scCO_2$ at T=36 ℃ and P=7.9 MPa. For the pure PEO, after $scCO_2$ exposure, the crystal structure seems to break up. When PEO composition was 80 %, PS molecules form island structures, whose size is almost identical to that annealed at 150 ℃. However, the crystalline structures are not clearly seen, while after the annealed condition. Increasing the mass ratio of PS, the phase separated structure becomes smaller after the CO_2 process than that observed after high temperature annealing. This indicates that $scCO_2$ can be used as a co-solvent to reduce the immiscibility. Further experiments are needed in the future. For the PEO/PS=80/20 film, we can see the big dendritic crystal structures at the film surface, as seen in the annealed films.

In Fig. 3-6, we compared the blend films after annealed at T=150 ℃ with the ones exposed to $scCO_2$ at T=50 ℃ and P=10 MPa. For pure PEO, the crystal of PEO becomes larger and smoother after the $scCO_2$ process. According to our previous experiments, the melting pressure of 50 nm thick pure PEO film in $scCO_2$ at T=50 ℃ is estimated to be 4 MPa. Hence, the $scCO_2$ condition used in the present study would melt the crystal and recrystallize during the rapid depressurization. In the case of 80 % PEO films, PS islands are formed in both situations, but the size of PS islands are somehow larger in $scCO_2$ than annealed condition. Interestingly, as shown in Fig. 3-3(i,n), the morphology of the PEO crystals is quite different from that after the high temperature annealing. The structure is similar to mass fractal structures due to the diffusion limited aggregation. In the morphologies of PEO/PS (50/50) blend films, large differences in the morphology between the two processes are observed (Fig. 3-3(o)). PS at the surface aggregate and form strip-like shape rather than round islands after exposed to $scCO_2$. In 20 % PEO, the surface morphologies are totally different from each other. After the $scCO_2$ process, there are no big crystal structures formed at the surface. The results imply that the PEO region swells significantly relative to the PS region. According to our previous experiments, the swelling ratios at the CO_2 condition are 0.3 for PS and 0.6 for PEO. Hence, the AFM

results are consistent with the swelling behavior. We believe that the bottom layer correspond to the PEO component. However, the crystalline structures of PEO may nucleate from the PEO/PS interface and form branched-like crystal structures. We are currently performing a series of experiments with different compositions to study the unique structures induced by the $scCO_2$ process.

Due to the huge crystal size in Fig. 3-2(d,l), we used optical microscope to measure the crystal. Fig. 3-4 shows the optical microscopy images for the 20 nm thick film (PEO/PS=20/80) after high temperature annealing (a) and exposed to $scCO_2$ at T=36 ℃ and P=7.9 MPa (b). Thus, after exposed to scCO2 at T=36 ℃ and P=7.9 MPa, the PEO crystal has more regular shape.

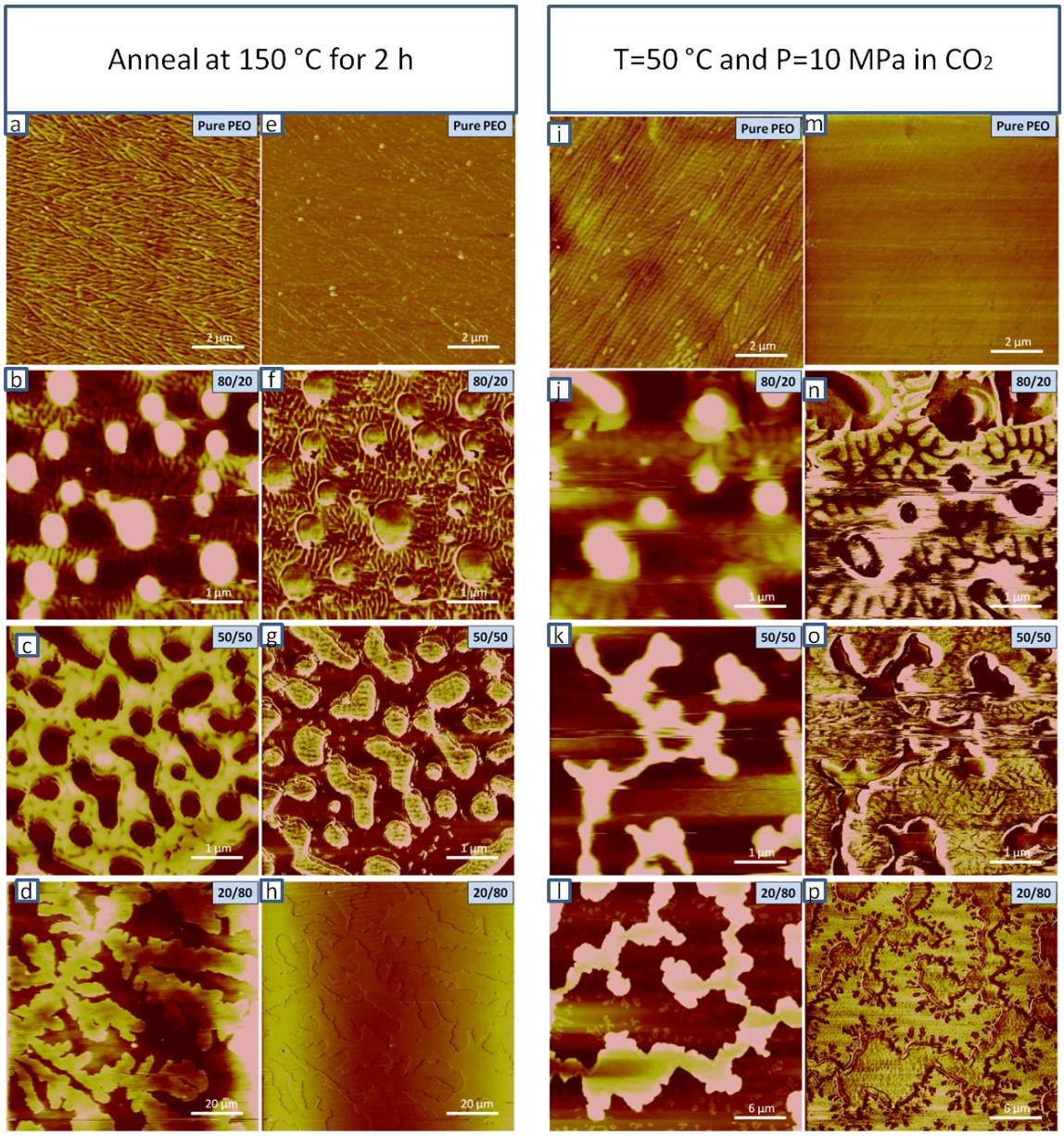

Fig. 3-3 Morphologies of 20nm ultrathin films in two conditions with four kinds of mass ratios. (a-d) PEO mass fractions are 100 %, 80 %, 50 %, 20 % respectively after annealing for 2 h fast quench. (e-h) Corresponding AFM friction images of (a-d). (i-l) PEO mass ratios are 100 %, 80 %, 50 %, 20 % respectively in the condition of $scCO_2$ at T=50 ℃ P=10 MPa. (m-p) Corresponding AFM friction images of (i-l).

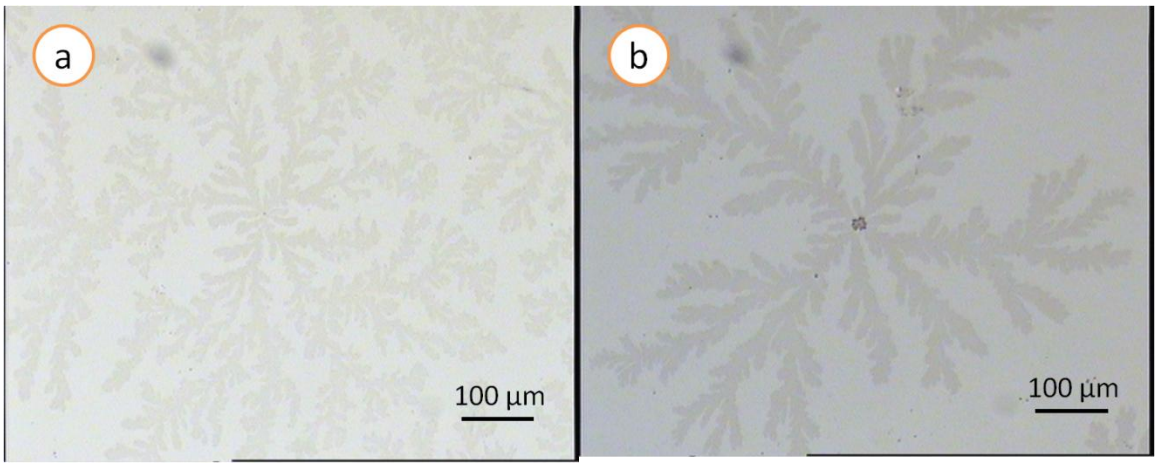

Fig. 3-4 Optical microscopy images of 20 nm 20 % PEO in two conditions: (a) annealed at 150 ℃ (b) exposed to $scCO_2$ at T=36 ℃ and P=7.9 MPa.

3.2.2 The effect of $scCO_2$ on the 50 nm PEO/PS blend films

We compare three different will processing conditions for the PEO/PS blend 50 nm thick films: (i) annealed at 150 ℃ for two 2 h; (ii) exposed to $scCO_2$ at T=36 ℃ and P=7.9 MPa for 2 h; (iii) exposed to $scCO_2$ at T=50 ℃ and P=10 MPa for 2 h.

Fig. 3-5 is the comparison of the film morphologies between the annealed film to $scCO_2$ treated film at T=36 ℃ and P=7.9 MPa. For the pure PEO, the crystal structure is nearly identical to each other. In the case of the 80 % PEO composition, PS islands are formed at the surface and no crystal structure is observed in both conditions. The 50 % PEO films do not show the clear crystal structures in both conditions. However, when the composition of PEO is 20 %, large crystals present at the film surface after the CO_2 process. The nuclei sites of the dendritic crystal seem to be PS, which is brighter in the height image (l). The clear crystal structures were not observed in the annealed films (PEO/PS=20/80).

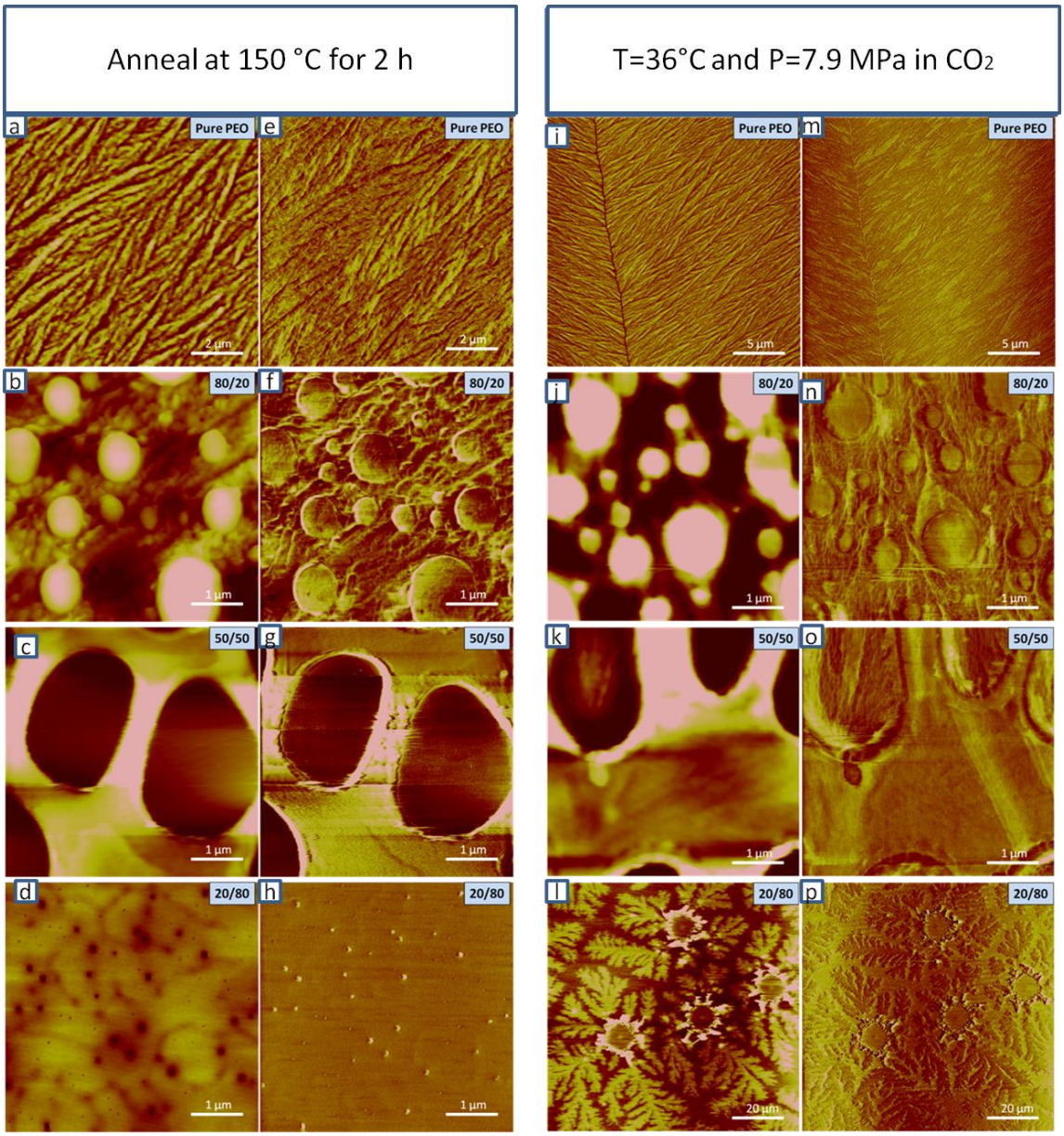

Fig. 3-5 Morphologies of the 50 nm PEO/PS blend films under the different processing conditions with four kinds of mass ratios. (a-d) PEO mass fractions are 100 %, 80 %, 50 %, 20 % respectively after annealed for 2 h fast quench. (e-h) Corresponding AFM friction images of (a-d). (i-l) mass ratios are 100 %, 80 %, 50 %, 20 % respectively exposed to $scCO_2$ at T=36 ℃ P=7.9 MPa. (m-p) Corresponding AFM friction images of (i-l).

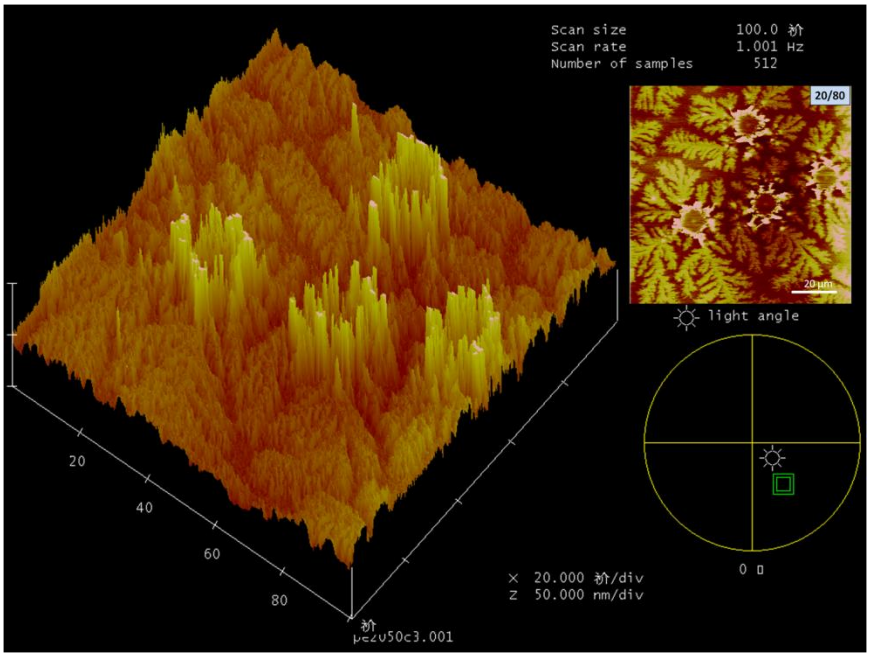

Fig. 3-6 Surface plot of 50 nm 20% PEO exposed in $scCO_2$ at T=36 ℃ and P=7.9 MPa

Fig. 3-6 is the surface plot image of the 50 nm thick film (PEO/PS=20/80) after the $scCO_2$ treatment at T=36 ℃ and P=7.9 MPa. From this image, we can see that the higher PS region form a rim-like structure, which is often seen in the phase-separation of polymer blend thin films. Therefore in the presence of the CO_2 solvent, PS could be the nuclei sites of PEO and induce dendritic crystal structures.

Fig. 3-7 shows the optical microscopic images for the 20 nm thick film after the $scCO_2$ process. Fig. 3-7(b) and (c) correspond to the region A and region C in (a), respectively, and Fig. 3-7(d) is the boundary between the regions. From images, we can see the similar morphology to the AFM results in the region B. This is the PEO-rich area, where PS aggregate as a rim-like structure and act as the nuclei site of the PEO dendritic crystal as seen in Fig. 3-7(c). On the other hand, the region A corresponds to the PS-rich region where PS is dispersed in PEO and the smaller PS islands induce smaller PEO crystal structures (Fig.3-7(b)). Fig.3-7(d) clearly shows the bounder between the two regions.

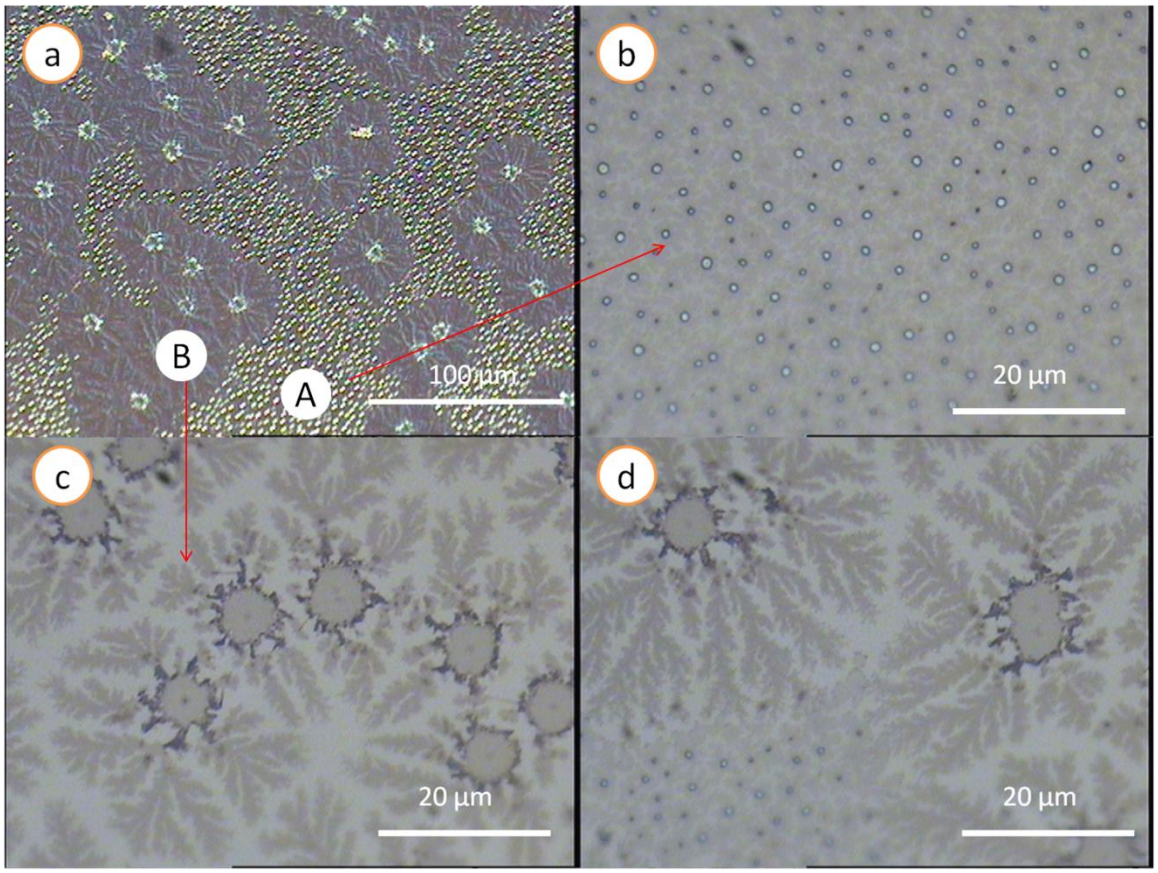

Fig. 3-7 Optical microscopy images of 20 nm 20 % PEO exposed in $scCO_2$ at T=36 ℃ and P=7.9 MPa of different sizes and positions. (b) Zoom in region B in (a). (c) Zoom in region A in (a). (c) Corresponding to the boundary of region A and region B.

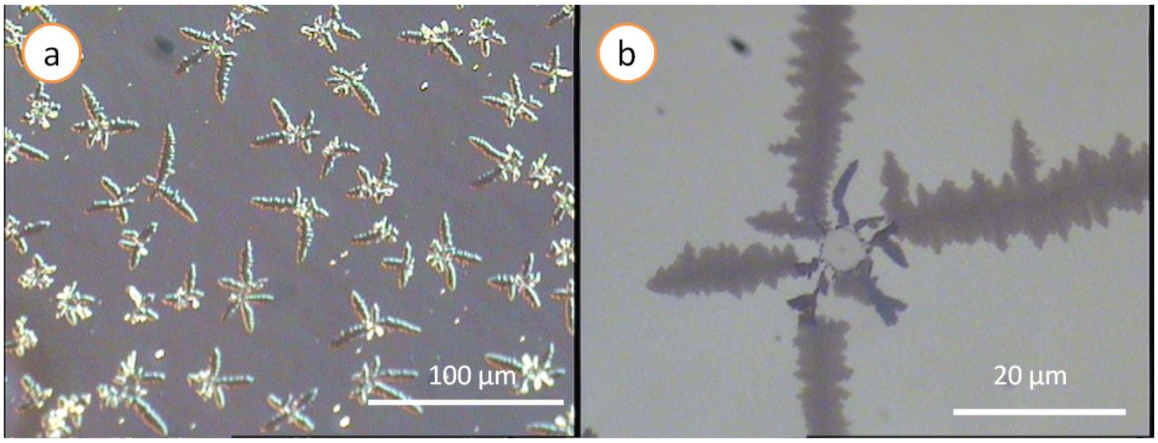

Fig. 3-8 Optical microscopy images of spin cast 20 nm thick film (PEO/PS=20/80) at different length scales.

Fig. 3-8 is the optical microscopy images for the spun-cast 20 nm thick film (PEO/PS=20/80). We measured the images to compare the crystal structure before and after $scCO_2$. From the comparison, we can see the morphologies are quite different. Just after spun cast, the crystal has the cross-like shape, while PEO recrystallizes to form the dendritic structures after the CO_2 process. The PS nuclei sites look like the same shape.

Fig. 3-9 is the comparison of the surface morphologies (50 nm thick films) between the annealed sample and the $scCO_2$ treated films at T=50 ℃ and P=10 MPa. For the pure PEO and 80 % PEO composition, the morphologies are nearly identical to each other. When the composition is symmetric, as shown in Fig. 3-9(k,o), the crystal structure is observed in the PEO domains, while the same film treated at T=36 ℃ and P=7.9 MPa did not show such crystal structures. Fig 3-10 shows the surface plot of the crystal structures in the PEO domains. When the PEO composition is 20 %, no dendritic crystal presents at the surface, while we can still see the higher rim structure of PS. We believe that in the presence of $scCO_2$ at T=50 ℃ and P=10 MPa, PEO would melt. By rapidly quenching the film to room temperature, we could preserve the melted structures (Fig.3-11). We are currently investigating the time-dependence of the non-equilibrium blend structures at room temperature.

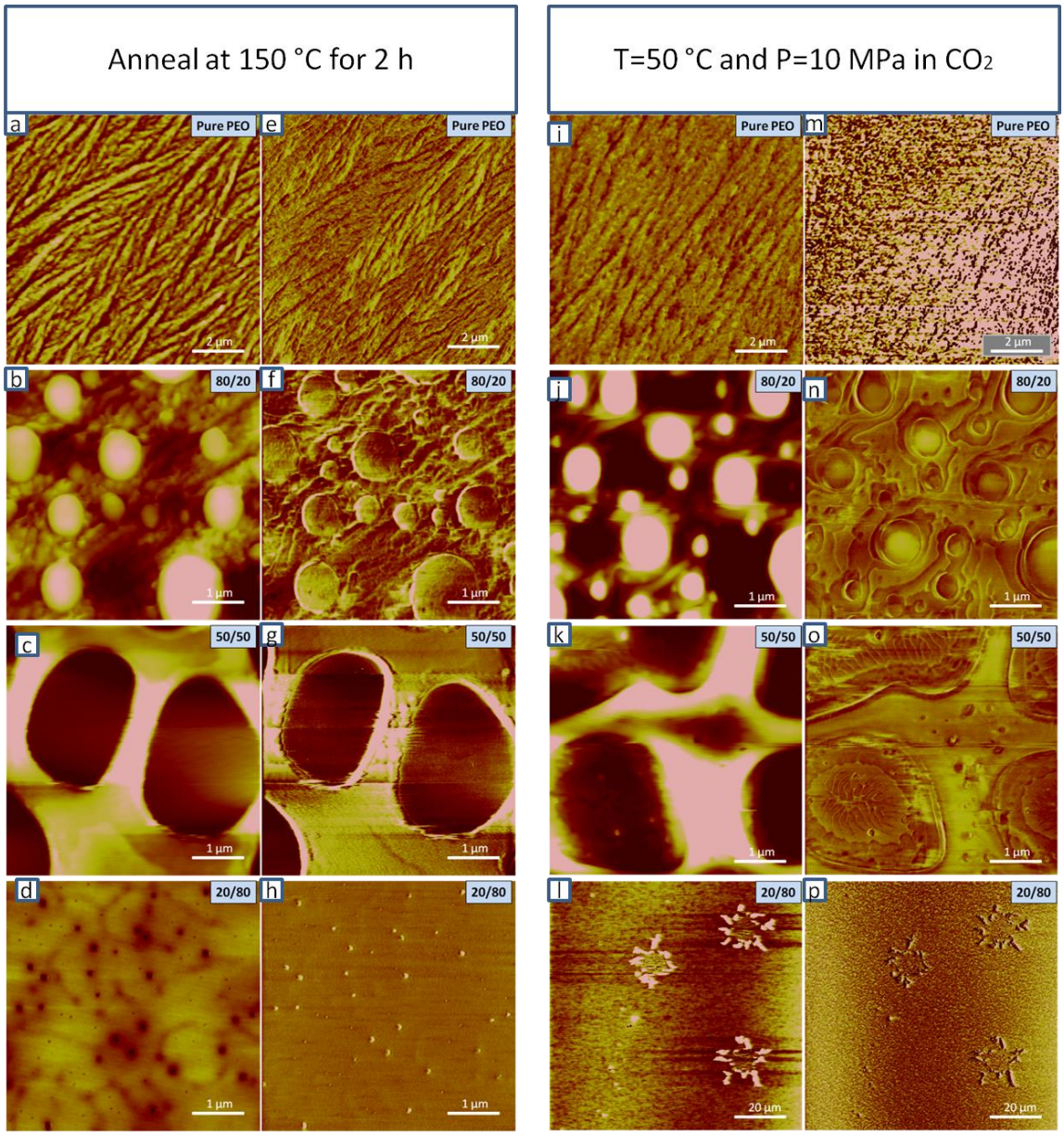

Fig. 3-9 Morphologies of 50nm ultrathin films in two conditions with four kinds of mass ratios. (a-d) PEO mass fractions are 100 %, 80 %, 50 %, 20 % respectively after annealing for 2 h fast quench. (e-h) Corresponding AFM friction images of (a-d). (i-l) mass ratios are 100 %, 80 %, 50 %, 20 % respectively after exposed to scCO$_2$ at T=50 ℃ P=10 MPa. (m-p) Corresponding AFM friction images of (i-l).

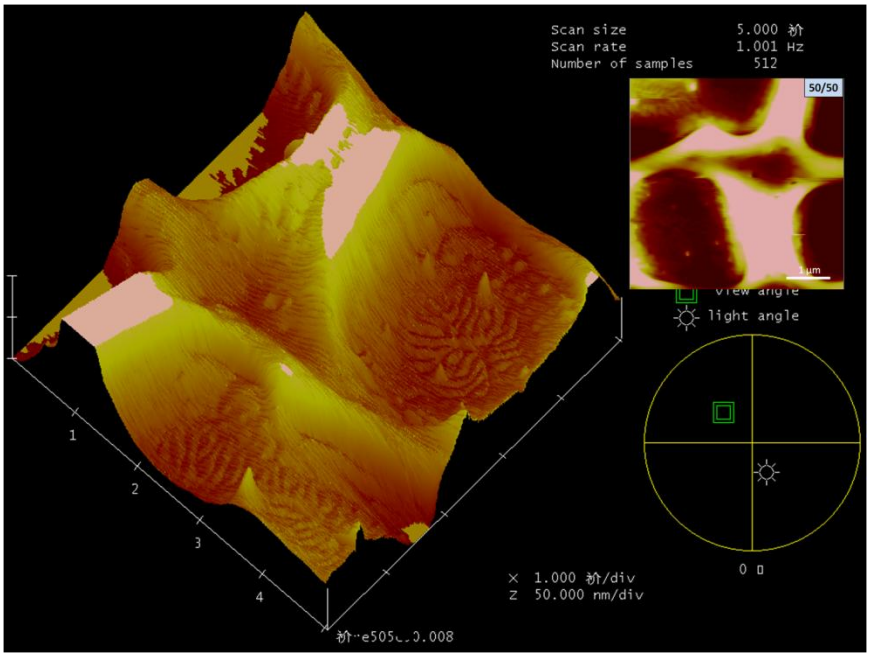

Fig. 3-10 Surface plot of 50 nm 50 % PEO exposed to $scCO_2$ at T=50 ℃ and P=10 MPa

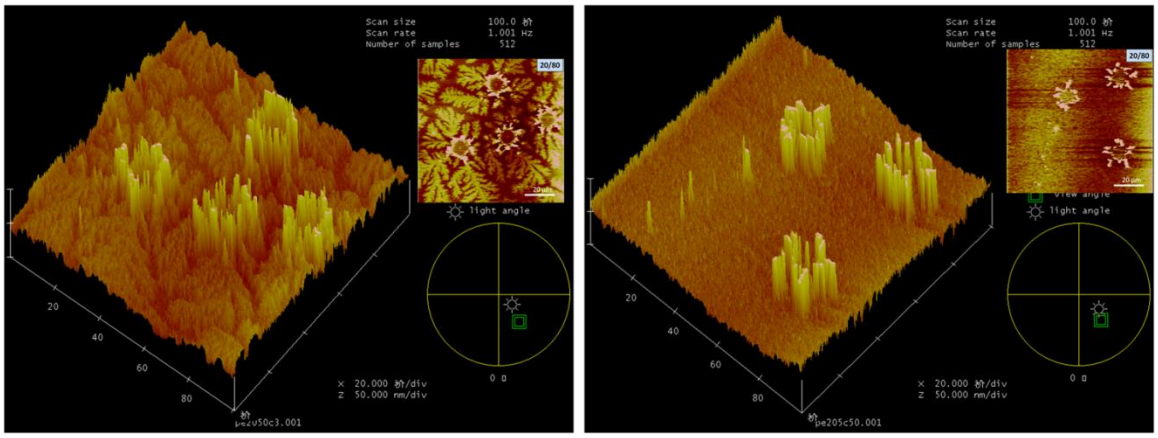

Fig. 3-11 Comparison of two surface plot of 50 nm 20% PEO exposed to $scCO_2$ at different ridge condition. Left one is at T=36 ℃ P=7.9 MPa, the right side is at T=50 ℃ P=10 MPa

Chapter 4: Conclusion and Future Work

In this research, we focus on the effect of $scCO_2$ on the PEO/PS blend thin films with different thicknesses (20 nm, 50nm) and mass ratios (100/0, 80/20, 50/50, and 20/80) by using AFM. We used two $scCO_2$ ridge conditions: T=36 ℃ and P=7.9 MPa, T=50 ℃ and P=10 MPa, where the anomalous plasticization effects have been reported. We found that the morphologies of the blend thin films alter significantly after the $scCO_2$ processes. At T=36 ℃ and P=7.9 MPa, PEO tends to form large dendritic structure, while at T=50 ℃ and P=10 MPa, PEO crystals are melted. We believe that due to the effect of density fluctuating $scCO_2$, polymer chain swells significantly, leading to the anomalous plasticization effect. Since the temperature of 50 ℃ is close to the bulk melting temperature of PEO (T_m=65 ℃), CO_2 can melt the PEO even below T_m. A series of the experiments elucidated that the plasticization effect is more remarkable in the 20 nm thick films than 50 nm thick films. This can be explained by the fact that the effect of density fluctuation is a surface effect, which occurs only near the CO_2/polymer interface. Especially, the surface morphologies of the 20 nm thick films are unique that can be seen only after the $scCO_2$ process.

In the future, we need to establish theories to explain the phenomena. To get more detailed structural information, we need X-ray reflectivity to measure the thickness and the density of the thin film and grazing incident X-ray diffraction to measure the crystal size and orientation of PEO.

References

(1) Singh, L. 3155344, Georgia Institute of Technology, 2004.
(2) Yang, J. P.; Liao, Q.; Zhou, J. J.; Jiang, X.; Wang, X. H.; Zhang, Y.; Jiang, S. D.; Yan, S. K.; Li, L. *Macromolecules* **2011**, *44*, 3511.
(3) Limary, R. 3114774, The University of Texas at Austin, 2002.
(4) Wang, H.; Composto, R. J. *The Journal of Chemical Physics* **2000**, *113*, 10386.
(5) Besancon, B. M. 3266790, The University of Texas at Austin, 2006.
(6) Ma, M.; He, Z.; Yang, J.; Wang, Q.; Chen, F.; Wang, K.; Zhang, Q.; Deng, H.; Fu, Q. *Langmuir : the ACS journal of surfaces and colloids* **2011**, *27*, 1056.
(7) BATES, F. S. *Science* **1991**, *251*, 898.
(8) Andersen, B. Thesis/dissertation, Manuscript, Halle (Saale), Univ., 2004.
(9) Yilmaz, E.; Yilmaz, O.; Caner, H. *European Polymer Journal* **1996**, *32*, 927.
(10) Singh, Y. P.; Singh, R. P. *European Polymer Journal* **1983**, *19*, 535.
(11) Virkar., P. A. In *notes of university of Utah. Spinodal Decomposition: Part 1: general description and practical implications*.
(12) Sirard, S. M. 3116397, The University of Texas at Austin, 2003.
(13) Hussain, Y. A. 3247040, North Carolina State University, 2006.
(14) Koga, T.; Jerome, J.; Rafailovich, M. H.; Chu, B.; Douglas, J.; Satija, S. *Advances in Colloid and Interface Science* **2006**, *128–130*, 217.
(15) Koga, T.; Seo, Y. S.; Shin, K.; Zhang, Y.; Rafailovich, M. H.; Sokolov, J. C.; Chu, B.; Satija, S. K. *Macromolecules* **2003**, *36*, 5236.
(16) Koga, T.; Seo, Y.-S.; Zhang, Y.; Shin, K.; Kusano, K.; Nishikawa, K.; Rafailovich, M. H.; Sokolov, J. C.; Chu, B.; Peiffer, D.; Occhiogrosso, R.; Satija, S. K. *Phys Rev Lett* **2002**, *89*, 125506.
(17) Alessi, P.; Cortesi, A.; Kikic, I.; Vecchione, F. *Journal of Applied Polymer Science* **2003**, *88*, 2189.
(18) Zhou, H.; Fang, J.; Yang, J.; Xie, X. *The Journal of Supercritical Fluids* **2003**, *26*, 137.
(19) Koga, T.; Jerome, J. L.; Seo, Y. S.; Rafailovich, M. H.; Sokolov, J. C.; Satija, S. K. *Langmuir : the ACS journal of surfaces and colloids* **2005**, *21*, 6157.
(20) Bailey, F. E. K., J. V. *Poly(Ehtylene Oxide)*; Academic Press: New York, 1976.
(21) Gu, X.; Wang, G. *Appl Surf Sci* **2011**, *257*, 1952.
(22) Hashmi, S. A.; Kumar, A.; Maurya, K. K.; Chandra, S. *Journal of Physics D: Applied Physics* **1990**, *23*, 1307.
(23) Mahato, R. I.; CRC Press, 2005: 2005, p 669 pages.
(24) Ferreiro, V.; Douglas, J. F.; Warren, J.; Karim, A. *Physical Review E* **2002**, *65*, 051606.
(25) Ma, M.; He, Z.; Yang, J.; Chen, F.; Wang, K.; Zhang, Q.; Deng, H.; Fu, Q. *Langmuir : the ACS journal of surfaces and colloids* **2011**, *27*, 13072.
(26) Jerome, L. J. 3206464, State University of New York at Stony Brook, 2005.
(27) Koga, T.; Akashige, E.; Reinstein, A.; Bronner, M.; Seo, Y. S.; Shin, K.; Rafailovich, M. H.; Sokolov, J. C.; Chu, B.; Satija, S. K. *Physica B: Condensed Matter* **2005**, *357*, 73.